## MISCELLANEOUS

# On the Mechanism of the Generation of Runaway Electrons after a Breakdown of a Gap

**D. V. Beloplotov[a], \*, V. F. Tarasenko[a, b], V. A. Shklyaev[a], and D. A. Sorokin[a]**

[a] *Institute of High Current Electronics, Siberian Branch, Russian Academy of Sciences, Tomsk, 634055 Russia*
[b] *National Research Tomsk State University, Tomsk, 634050 Russia*
*\*e-mail: rff.qep.bdim@gmail.com*

Data that explain the generation of runaway electrons after the breakdown of a gap with a sharply inhomogeneous distribution of the electric field strength are presented. Using a special technique for measuring a displacement current caused by the appearance and propagation of a streamer, the voltage and current waveforms of runaway electrons have been synchronized to each other, as well as to the dynamics of the streamer formation, which has been recorded using a four-channel ICCD camera. It is shown that the first runaway electron beam is generated near the pointed cathode at the time when the streamer appears. The second runaway electron beam is generated at the time when a backward ionization wave reaches the pointed cathode. It is assumed that the generation of the second runaway electron beam occurs in the cathode layer. This is confirmed by the fact that the second runaway electron beam does not appear in those discharge implementations at which the cathode spot is observed before the gap is bridged by the plasma.

### INTRODUCTION

A nanosecond gas discharge, as an efficient tool to generate a low-temperature plasma, attracts worldwide attention. It can be used to sterilize medical instruments, food, and packing products; purify exhaust gases and wastewater; and process the surfaces of metals, semiconductors, insulators, and living tissues [1]. The wide possibilities of using the nanosecond discharge plasma are due to the variety of chemically active types of atoms and molecules formed during ionization, excitation, dissociation, and recombination.

The formation of nanosecond gas discharges is often accompanied by the generation of runaway electrons (REs). The effect is especially pronounced in the discharges formed under high overvoltage. This is ensured by the use of gaps with a sharply inhomogeneous distribution of the electric field strength and a nanosecond duration of high-voltage pulses. The role of REs in the formation of discharges, including atmospheric discharges, is being actively discussed again in connection with the development of both theoretical models and measuring techniques [2–14]. Thus, it was shown in recent theoretical studies that REs are capable of providing preliminary gas ionization ahead of the front of a negative streamer formed in air at atmospheric pressure disregarding photoionization [3]. It was found in experimental studies that REs can be generated not only in the pre-breakdown stage of the discharge but also after the breakdown of the gap at the voltage drop [15]. In this case, two RE current pulses with durations of about 0.1 and 0.3 ns, respectively, were observed, and the delay between them was 1 ns. It is assumed that the generation of the second pulse occurs during the propagation of secondary ionization waves. Double RE current pulses were also observed recently in [16] at the voltage across the gap an order of magnitude higher and at the air pressure ≈4 times higher than those in [15]. The delay between RE current pulses was ≈0.15 ns. It is assumed that the generation of the second flow of REs occurs in the partially ionized gap after the passage of the first flow of REs. Earlier, the generation of double RE current pulses was also observed in [17, 18].

In this work, we attempt to reveal the mechanism of the generation of the second RE beam under conditions (voltage, gas pressure, gap) similar to those in [15]. To this end, the formation of the discharge was studied using high-speed shooting methods, as well as using a new method for studying the discharge by measuring a displacement current caused by the streamer motion [19]. This method was used to determine when the generation of REs occurs with respect to the dynamics of a negative streamer formed in air at atmospheric pressure [20]. Thus, the aim of this work is to determine the mechanism of the generation of REs after bridging the gap by the plasma.
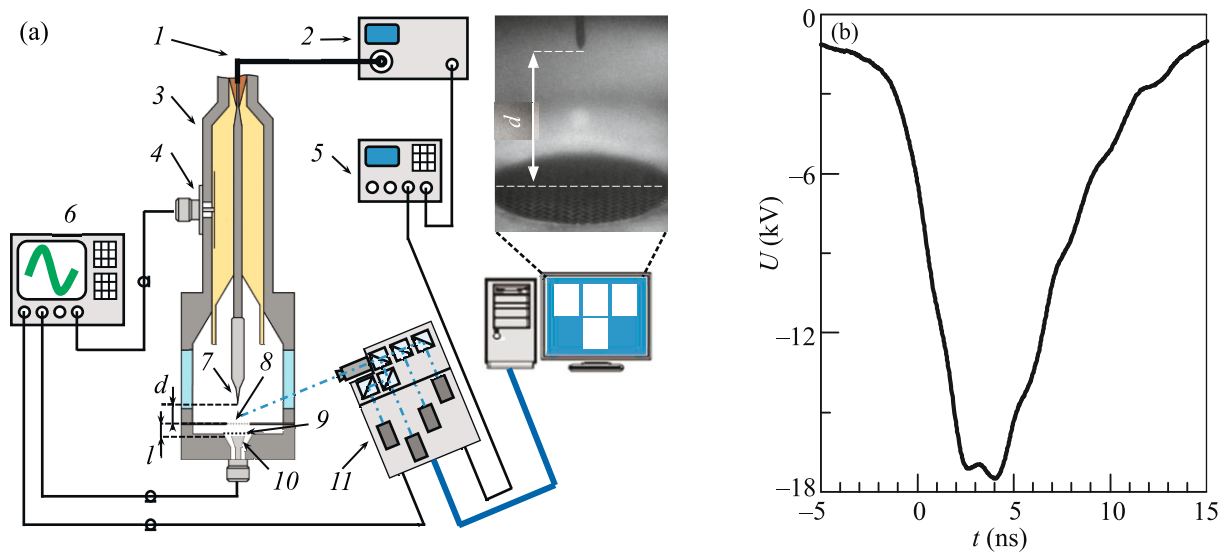
**Fig. 1.** (Color online) (a) Layout of the experimental setup: (*1*) high-voltage cable, (*2*) high-voltage nanosecond generator, (*3*) coaxial transmission line, (*4*) capacitive voltage divider, (*5*) start generator, (*6*) oscilloscope, (*7*) high-voltage electrode, (*8*) grounded electrode (grid), (*9*) grid, (*10*) collector, (*11*) ICCD camera. (b) Waveform of the voltage pulse at a matched load.

## EXPERIMENTAL SETUP AND MEASUREMENT TECHNIQUES

The experiments were carried out on a setup consisting of a gas-discharge chamber combined with a transmission line ($Z = 75\ \Omega$), an NPG-18/3500N generator of high-voltage nanosecond pulses, a LeCroy WaveMaster 30Zi (16 GHz, 20 GS/s) oscilloscope, and an HSFC-PRO four-channel ICCD camera. The layout of the experimental setup and the waveform of the voltage pulse at the matched load are shown in Fig. 1.

Voltage pulses were applied to the input of the transmission line using a high-voltage coaxial cable 3 m long with a characteristic impedance of 75 $\Omega$. The voltage pulses were recorded using a capacitive voltage divider installed in the transmission line. The voltage across the gap was recovered from the incident (Fig. 1b) and reflected waves. A high-voltage electrode 5 mm long was made of a sewing needle with a base diameter of 1 mm and a radius of curvature of the needle tip of 75 μm. The grounded electrode was flat with a hole in the center 1 cm in diameter. A perforated grid with a transmittance of 0.75 was installed in the hole. The hole edge was rounded and polished in order to eliminate the nonuniformity of the electric field distribution at the edge−grid interface. This made it possible to avoid the closure of the discharge channel to the edge. The distance between the electrodes was 8.5 mm.

The RE current $I_{RE}$ was measured using a collector located behind the grounded grid electrode. A grid with a transmittance of 0.3 was located in front of the receiving part of the collector (see Fig. 1a). This made it possible to exclude the effect of the electric field

passing through the grounded grid electrode. However, in the absence of a grid in front of the receiving part of the collector, it is possible to simultaneously measure the RE current $I_{RE}$ and dynamic displacement current $I_{DDC}$ caused by the redistribution of the electric field in the main gap during the formation of the plasma [19]. From the waveform of the dynamic displacement current $I_{DDC}$, it can be determined with high accuracy at what time the streamer appeared and when it reached the flat grounded electrode [19]. Having the sum of two signals $I_{RE}$ and $I_{DDC}$, one can accurately determine when the generation of REs occurs [20].

The development of plasma emission in the gap was studied using a four-channel ICCD camera. This camera produces four consecutive images with a known delay with respect to each other per one implementation. The minimum exposure time for one frame is 3 ns. In the experiment, the exposure time was 3 ns for three channels and 20 ns for the fourth channel. Thus, the first three channels (C1−C3) made it possible to study the dynamics of the discharge formation, and the fourth channel (C4) allowed obtaining an integral image of plasma emission per one implementation. In this case, channel C1 at the time of switching on formed a sync signal, which was recorded by the oscilloscope simultaneously with the signals from the capacitive voltage divider and the collector. This made it possible to synchronize the ICCD images and the voltage and current waveforms of REs.

In a separate series of experiments, the dynamic displacement current $I_{DDC}$, caused by the redistribution of the electric field strength in the gap during the
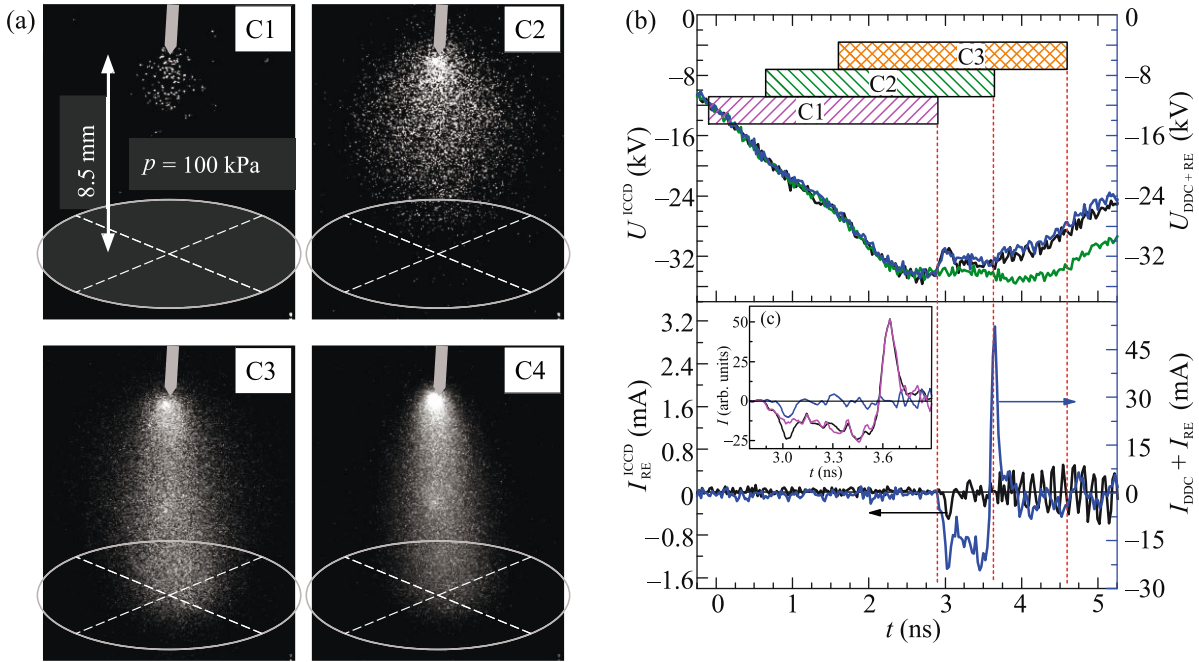
**Fig. 2.** (Color online) (a) Images of discharge plasma emission in air at a pressure of 100 kPa. (b) Voltage, $U^{\text{ICCD}}$, and current, $I_{\text{RE}}^{\text{ICCD}}$, waveforms of runaway electrons recorded during experiments with the four-channel ICCD camera, and voltage, $U_{\text{DDC+RE}}$, and current, $I_{\text{RE}}$, waveforms of runaway electrons with the dynamic displacement current $I_{\text{DDC}}$ recorded in a separate experiment. The green curve is the no-load voltage waveform. (c) $I_{\text{RE}}^{\text{ICCD}}$ and $I_{\text{RE}} + I_{\text{DDC}}$ current waveforms of runaway electrons and the difference of these signals. C1, C2, C3, and C4 are the channel numbers of the ICCD camera. The rectangles show the moments of switching on the camera channels. The length of the rectangles corresponds to the duration of the exposure.

formation and propagation of the streamer, and the RE current $I_{\text{RE}}$ were measured using the collector. As a result, the current waveforms of REs were synchronized with the voltage across the gap, reconstructed from the incident and reflected waves.

The gas discharge chamber was evacuated with a forevacuum pump and then filled with air. The pressure was varied in the range of 12–100 kPa.

## RESULTS AND DISCUSSION

The formation of a streamer with a large diameter was observed at the air pressure of 100 kPa (Fig. 2), as in previous studies [2, 4, 15, 19]. The characteristic features of the dynamics of the formation of such streamer are the high velocity of the streamer at the start and before reaching the opposite electrode [21], as well as the flow of a noticeable current in the external circuit during the formation of the streamer, the value of which is proportional to its velocity. We call this current the dynamic displacement current to emphasize that it is due to the redistribution of the electric field in the gap caused by the formation of a streamer rather than to the external change in the electrode potentials [19]. In addition, the appearance and formation of a streamer (Fig. 2a) is accompanied by the voltage drop across the gap (Fig. 2b), since the cur-

rent is already flowing in the external circuit. This effect was also described theoretically [22, 23]. The higher the streamer velocity, the stronger the voltage drop (see voltage waveforms in Figs. 2–4).

The dynamic displacement current $I_{\text{DDC}}$ can be measured with a collector located behind the grounded grid electrode (Fig. 1). This is possible because the electric field penetrates through the grid with a large (about four orders of magnitude [20]) attenuation. The $I_{\text{DDC}}$ waveform can be used to determine the time of the appearance of the streamer (the rise of $I_{\text{DDC}}$, Figs. 2b, 2c) and the time of when it reaches the opposite grid electrode (polarity reversal of $I_{\text{DDC}}$, Figs. 2b, 2c), and it is also possible to determine the time of the generation of REs with respect to the streamer dynamics [20]. In addition, the electric field strength $E_c(t)$ can be calculated near the grid electrode in absolute units [19].

Figure 2b shows the RE current waveform $I_{\text{RE}}^{\text{ICCD}}$ measured in the experiment using the ICCD camera and the waveform of the sum $I_{\text{RE}} + I_{\text{DDC}}$ measured in a separate experiment. It should be noted that $\sim 10^2$ waveforms were recorded in each experiment, and then the cases with the same breakdown delay time were selected. It is seen that, if the ionization pro-
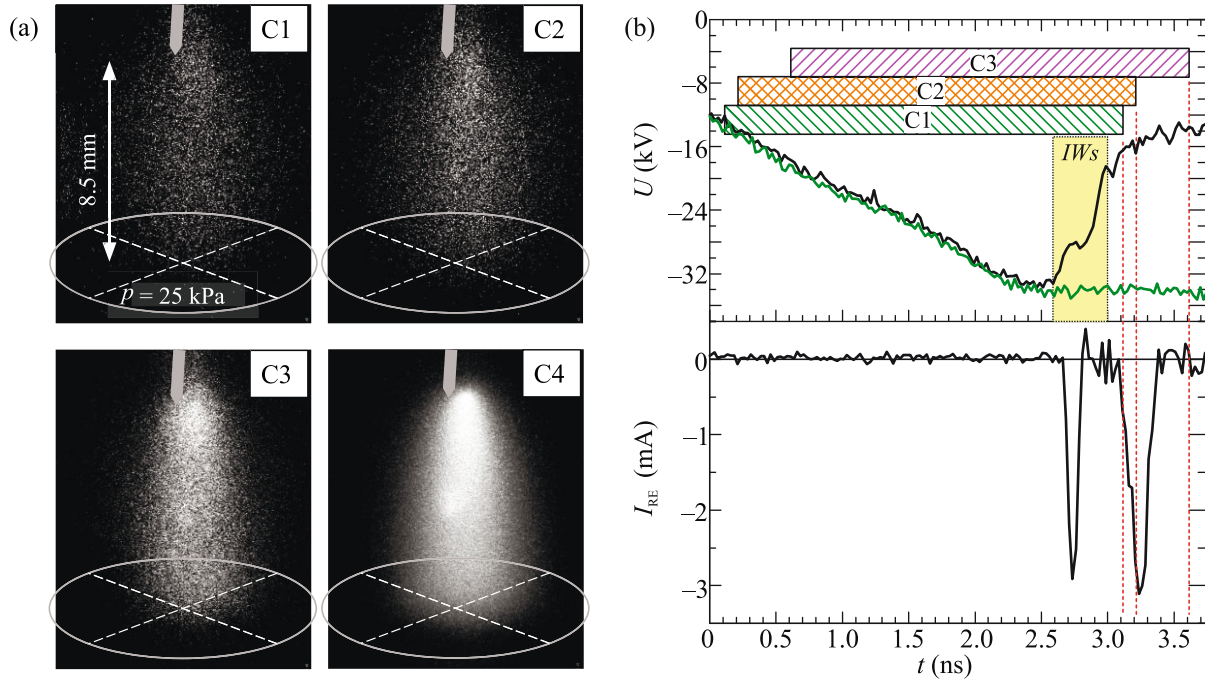
**Fig. 3.** (Color online) (a) Images of discharge plasma emission in air at a pressure of 25 kPa. (b) Corresponding voltage, $U$, and current, $I_{RE}$, waveforms of runaway electrons. The green curve is the no-load voltage waveform in the open mode. C1, C2, C3, and C4 are the channel numbers of the ICCD camera. The rectangles show the time of switching on the camera channels. The length of the rectangles corresponds to the duration of the exposure. Forward and backward ionization waves are marked as *IWs*. The figure corresponds to the case where the cathode spot is absent at the initial stage of the discharge.

cesses start under the same voltage conditions in two different experiments, then the dynamics of the discharge formation is reproduced (Fig. 2a, $U^{ICCD}$ and $U_{DDC+RE}$). This makes it possible to synchronize the RE current $I_{RE}^{ICCD}$ to the voltage across the gap $U^{ICCD}$ and to the dynamics of the streamer formation shown in Fig. 2a.

Figures 2b and 2c shows that the RE current pulse is recorded by the collector $\approx 80$ ps later than the beginning of the current $I_{DDC}$. However, it is necessary to take into account that the velocity of REs with the energy $\approx 35$ keV is less than the propagation velocity of the electromagnetic wave causing the signal $I_{DDC}$. The estimates that took into account the distribution of the electric field strength in the gap without plasma show that REs generated near the cathode reach the collector $\approx 75$ ps later than the electromagnetic wave caused by the appearance of the plasma near the cathode. The energy distribution of electrons was not taken into account. Thus, the RE current pulse should be shifted $\approx 75$ ps to the left, which corresponds to the time of the generation of REs with respect to the streamer appearance. It follows that REs are generated directly at the start of ionization processes near the cathode. The FWHM duration of the RE current pulse is $\approx 77$ ps.

The time point when the polarity of $I_{DDC}$ changes (Figs. 2b, 2c) corresponds to reaching the maximum of $E_c(t)$. Then, $E_c(t)$ decreases because of the gas ionization near the grid surface and the redistribution of the electric field strength occurs. We believe that a backward ionization wave is formed during this stage. In [21], the characteristic propagation of the emission front in the opposite direction was observed in images obtained with a streak camera. The data obtained for $\sim 10^2$ pulses under different conditions show that the backward ionization wave is formed always.

Figure 3 shows the ICCD images of the discharge plasma emission, as well as the corresponding voltage and current waveforms of REs at an air pressure of 25 kPa. The time of switching on and the exposure duration of the ICCD channels of the camera C1−C3 are shown by rectangles in Fig. 3b.

It should be noted that, regardless of pressure, the breakdown most often occurred when the voltage reached a plateau. It can be seen that two RE current pulses are observed under these conditions. The second RE current pulse is recorded when the voltage across the gap drops. The RE current waveforms were synchronized to the voltage waveforms by the method described above. However, to determine the time of the generation of each RE beam, it is necessary to take into account the time of flight of electrons from the generation zone to the collector. The first RE beam is
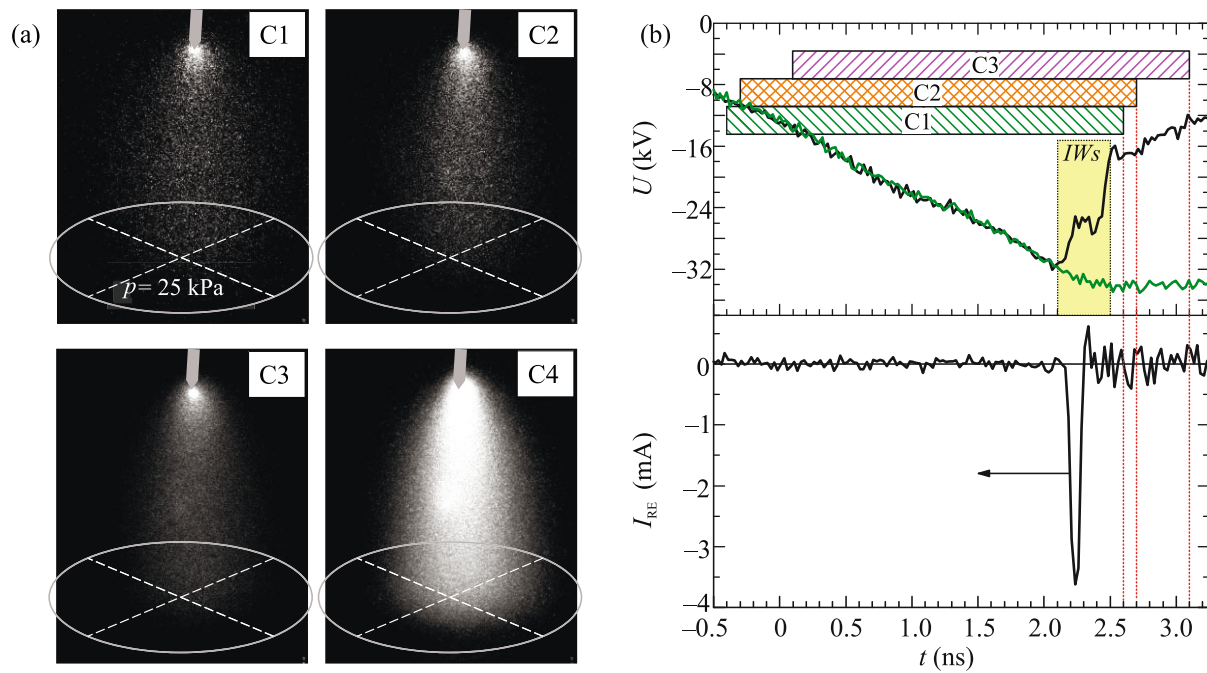
**Fig. 4.** (Color online) (a) Images of discharge plasma emission in air at a pressure of 25 kPa. (b) Corresponding voltage, $U$, and current, $I_{RE}$, waveforms of runaway electrons. The green curve is the no-load voltage waveform. C1, C2, C3, and C4 are the channel numbers of the ICCD camera. The rectangles show the moments of switching on the camera channels. The length of the rectangles corresponds to the duration of the exposure. Forward and backward ionization waves are marked as *IWs*. The figure corresponds to the case where the cathode spot was formed during bridging the gap by the plasma.

generated near the cathode at the start of ionization processes. As already stated above, the RE current pulse should be shifted to the left by $\approx 75$ ps, which corresponds to the time of the generation of REs. The second beam is presumably generated in the cathode layer after the backward ionization wave reaches the cathode. The second sharp voltage drop corresponds to the propagation of the backward ionization wave in the gap (Fig. 3b). The second RE beam is generated at the voltage across the gap from $-20$ to $-15$ kV. The time of flight of electrons from the cathode to the collector is $\approx 100$ ps at this voltage. The energy distribution of electrons was disregarded.

Apparently, when the front of the backward ionization wave approaches the cathode, the reduced electric field strength $E/p$ in the cathode layer increases sharply and exceeds the critical value $(E/p)_{cr}$ necessary for the transition of a significant part of the electrons into the continuous acceleration mode. In addition, the field emission current from the cathode should increase sharply. Acquiring a high energy in the cathode layer, electrons can continue to accelerate in the plasma channel, since, as known, the quantity $(E/p)_{cr}$ decreases with increasing electron energy.

The cathode layer can disappear because of the explosion of microprotrusions on the cathode surface and the formation of a cathode spot. It can be seen in Fig. 3a that the cathode spot is absent at the initial stage of the discharge. However, the cathode spot is observed only in the image obtained for the entire pulse (Fig. 3a, frame C4).

The cathode spot can be formed when the streamer (the first ionization wave) reaches the anode (Fig. 2) or when the backward ionization wave reaches the cathode (Fig. 4). Only one RE current pulse was observed in such variants of the implementation of the discharge as shown in Fig. 4.

The generation of two RE beams was observed in almost every pulse at an air pressure of 12 kPa. In addition, implementations of the discharge were observed when only the second RE beam was generated. The feature of the formation of the discharge at a given pressure was that the plasma was adjacent not only to the tip of the needle but also to its lateral surface, the area of which is one or two orders of magnitude larger. In this case, at a comparable discharge current (300–400 A), the current density at the cathode $j$ was one or two orders of magnitude lower, which increases the formation time $t_f$ of the cathode spot by at least two orders of magnitude ($j^2 t_f = \text{const}$ [24]).

## CONCLUSIONS

The data obtained in this work have shown that runaway electrons can be generated at fairly low (tens of kilovolts) voltages across the gap with a sharply

nonuniform distribution of the electric field strength. The presence of the cathode layer can provide the generation of runaway electrons even after the bridging of the gap by the plasma of the first ionization wave. In this case, the amplitude and duration of the runaway electron current pulse is larger than those of the runaway electron current pulse generated in the pre-breakdown stage of the discharge. The fast transition to explosive electron emission limits the generation of the second runaway electron beam. The data obtained expand the understanding of the generation of runaway electrons. For example, the generation of runaway electrons can be expected under conditions where the distribution of the electric field strength is uniform, but the formation of a cathode layer is possible.

## REFERENCES

1. K.-D. Weltmann, J. F. Kolb, M. Holub, D. Uhrlandt, M. Šimek, K. Ostrikov, S. Hamaguchi, U. Cvelbar, M. Černák, B. Locke, A. Fridman, P. Favia, and K. Becker, Plasma Process Polym. **16**, 1800118 (2018).

2. G. V. Naidis, V. F. Tarasenko, N. Yu. Babaeva, and M. I. Lomaev, Plasma Sources Sci. Technol. **27**, 013001 (2018).

3. N. Y. Babaeva, G. V. Naidis, D. V. Tereshonok, and E. E. Son, J. Phys. D: Appl. Phys. **51**, 434002 (2018).

4. V. F. Tarasenko, G. V. Naidis, D. V. Beloplotov, D. A. Sorokin, M. I. Lomaev, and N. Yu. Babaeva, Plasma Phys. Rep. **46**, 320 (2020).

5. V. Tarasenko, Plasma Sources Sci. Technol. **29**, 034001 (2020).

6. A. V. Kozyrev, E. M. Baranova, V. Yu. Kozhevnikov, and N. S. Semenyuk, Tech. Phys. Lett. **43**, 804 (2017).

7. V. Y. Kozhevnikov, A. V. Kozyrev, N. S. Semeniuk, and A. O. Kokovin, IEEE Trans. Plasma Sci. **46**, 3468 (2018).

8. V. A. Shklyaev, E. Kh. Baksht, S. Ya. Belomyttsev, A. G. Burachenko, and A. A. Grishkov, J. Appl. Phys. **121**, 093304 (2017).

9. V. A. Shklyaev, E. Kh. Baksht, S. Ya. Belomyttsev, A. G. Burachenko, A. A. Grishkov, and V. F. Tarasenko, J. Appl. Phys. **118**, 213301 (2015).

10. G. S. Diniz, C. Rutjes, U. Ebert, and I. S. Ferreira, J. Geophys. Res. Atmos. **124**, 189 (2019).

11. D. Sarria, C. Rutjes, G. Diniz, A. Luque, K. M. A. Ihaddadene, J. R. Dwyer, N. Ostgaard, A. B. Skeltved, I. S. Ferreira, and U. Ebert, Geosci. Model Dev. **11**, 4515 (2018).

12. S. Nijdam, J. Teunissen, and U. Ebert, Plasma Sources Sci. Technol. **29**, 103001 (2020).

13. N. M. Zubarev, G. A. Mesyats, and M. I. Yalandin, JETP Lett. **105**, 537 (2017).

14. G. A. Mesyats and M. I. Yalandin, Phys. Usp. **62**, 699 (2019).

15. V. F. Tarasenko, D. V. Beloplotov, M. I. Lomaev, and D. A. Sorokin, Plasma Sci. Technol. **21**, 044007 (2019).

16. N. Zubarev, K. Sharypov, S. Shunailov, A. Sadykova, V. Shpak, and M. Yalandin, in *Proceedings of the 7th International Congress on Energy Fluxes and Radiation Effects EFRE-2020, Tomsk, Russia* (2020), p. 364.

17. E. Kh. Baksht, V. F. Tarasenko, M. I. Lomaev, and D. V. Rybka, Tech. Phys. Lett. **33**, 373 (2007).

18. A. V. Gurevich, G. A. Mesyats, K. P. Zybin, A. G. Reutova, V. G. Shpak, S. A. Shunailov, and M. I. Yalandin, Phys. Lett. A **375**, 2845 (2011).

19. D. V. Beloplotov, M. I. Lomaev, V. F. Tarasenko, and D. A. Sorokin, JETP Lett. **107**, 606 (2018).

20. D. V. Beloplotov, V. F. Tarasenko, M. I. Lomaev, and D. A. Sorokin, IEEE Trans. Plasma Sci. **47**, 4521 (2019).

21. D. A. Sorokin, V. F. Tarasenko, D. V. Beloplotov, and M. I. Lomaev, J. Appl. Phys. **125**, 143301 (2019).

22. S. Ya. Belomyttsev, A. A. Grishkov, V. A. Shklyaev, and V. V. Ryzhov, J. Appl. Phys. **123**, 203302 (2018).

23. S. Ya. Belomyttsev, A. A. Grishkov, V. A. Shklyaev, and V. V. Ryzhov, J. Appl. Phys. **123**, 043309 (2018).

24. S. P. Bugaev, E. A. Litvinov, G. A. Mesyats, and D. I. Proskurovskii, Sov. Phys. Usp. **18**, 51 (1975).

*Translated by L. Mosina*